RESEARCH ARTICLE
SOLID EARTH: GEOELECTROMAGNETICS

Earth and Planetary Physics
9: 607–613, 2025
doi: 10.26464/epp2025040

Inverting tidal velocity from geomagnetic satellite by nonlinear method

Yu Gu[1,2,3], ZhengYong Ren[1,2,3*], Yang Wu[1,2,3], LiNan Xu[5], PengFei Liu[4], and Keke Zhang[4]

[1]State Key Laboratory of Critical Mineral Research and Exploration, Central South University, Changsha 410083, China;

[2]School of Geosciences and Info-Physics, Central South University, Changsha 410083, China;

[3]Key Laboratory of Metallogenic Prediction of Nonferrous Metals and Geological Environment Monitoring Ministry of Education, Central South University, Changsha 410083, China;

[4]Macau Institute of Space Technology and Application, Macau University of Science and Technology, Macao 999078, China;

[5]Institute of Earth Sciences, University of Lausanne, Lausanne 1015, Switzerland

Key Points:

- A nonlinear inversion method was developed to recover tidal velocities directly from satellite-observed tidal-induced magnetic fields, overcoming limitations of traditional altimetry-based approaches.
- The method demonstrated high accuracy in synthetic tests and good agreement with HAMTIDE model at mid-low latitudes using MSS-1, Swarm, CryoSat data.
- MSS-1's unique low-inclination orbit significantly improved resolution of tidal velocity model at mid-low latitudes through enhanced spatial coverage and east-west sensitivity.

Citation: Gu, Y., Ren, Z. Y., Wu, Y., Xu, L. N., Liu, P. F., and Zhang, K. (2025). Inverting tidal velocity from geomagnetic satellite by nonlinear method. *Earth Planet. Phys.*, *9*(3), 607–613. http://doi.org/10.26464/epp2025040

Abstract: This study presents an inversion method to recover the tidal flow velocity using tidal signals extracted from geomagnetic satellite dataset. By integrating the latest Earth conductivity profile and the Earth's magnetic field model, the limited memory quasi-Newton method (L-BFGS) is used to directly invert seawater flow velocities. We used the radial component of the induced magnetic field as the observed data, constructed an L_2-norm-based data misfit term using theoretical response and observed data, and applied smoothness constraints to the ocean flow velocity. The results agree well with the widely used HAMTIDE model in low- and mid-latitude regions, which is attributed to Macau Science Satellite-1's (MSS-1) unique low-inclination orbit of full coverage in these areas. These findings underscore MSS-1's potential to advance research on tidal-induced magnetic fields and their applications in ocean dynamics studies.

Keywords: Macau Science Satellite-1; satellite magnetic data; tidal velocity inversion

1. Introduction

Tides arise from gravitational variations induced by the celestial bodies, such as the Sun and Moon (Knauss and Garfield, 2016). These forces create periodic water movements with distinct cycles, such as the principal lunar semidiurnal constituent M2 (about 12.42 hours), the larger lunar elliptic semidiurnal constituent N2 (about 12.66 hours), and the principal lunar diurnal constituent O1 (about 25.82 hours). Tides play important roles on numerous scientific and practical studies, such as marine ecosystem dynamics, global climate regulation, economic development, and geomagnetic field modeling (Ray and Mitchum, 1997; Egbert and Ray, 2001; Grayver et al., 2017; Zhao ZX, 2023).

First author: Y. Gu, gycsu2021@csu.edu.cn
Correspondence to: Z. Y. Ren, renzhengyong@csu.edu.cn
Received 23 FEB 2025; Accepted 16 APR 2025.
First Published online 21 APR 2025.

Recent studies have mainly used tidal magnetic signals to study Earth's deep electrical structure. Using the extracted M2, N2, and O1 tidal-induced magnetic signals, inversion analyses have been performed to derive new theoretical one-dimensional (1D) and three-dimensional (3D) conductivity models of Earth's deep interior (Grayver et al., 2016, 2017; Šachl et al., 2022; Šachl et al., 2024). These models, in conjunction with improved tidal signal extraction, have advanced geomagnetic modeling, contributing to the development of widely used models such as CM6, CHAOS7, IGRF-13 and MGFM (Finlay et al., 2020; Sabaka et al., 2020; Alken et al., 2021; Yao HB et al., 2025).

The previous studies primarily focus on imaging subsurface electrical conductivity using induced magnetic fields, while lacking the application of magnetic fields for source inversion, particularly the inversion of ocean flow velocities. Measuring ocean flow patterns is a critically important field, and using satellite magnetic data to monitor seawater movement offers significant potential. To date, ocean flow velocity modeling has primarily relied on

satellite altimetry-derived sea surface height (SSH) measurements (Mazzega, 1985; Ray and Mitchum, 1997; Griffiths and Peltier, 2009; Ray and Zaron, 2011). Tide models such as HAMTIDE and TPXO, which are based on SSH data, have achieved high accuracy in estimating shallow-water tidal flows. However, their ability to characterize deep-ocean tidal currents remains limited due to the diminishing sensitivity of SSH measurements with increasing depth (Wunsch and Stammer, 1998). With their sensitivity to deep tidal motions, tidal-induced magnetic fields offer a promising alternative for velocity inversion. Despite this potential, applying electromagnetic data from ground-based observatories and geomagnetic satellites for tidal velocity modeling remained largely confined to theoretical discussions (Schnepf et al., 2014; Sabaka et al., 2016). In recent years, using a Kalman filtering approach, Saynisch et al. (2023) utilized data from CHAMP and Swarm for tidal velocity inversion. However, the results showed discrepancies of approximately 30% compared to HAMTIDE in shallow-water regions. Currently, the inversion of tidal-induced magnetic field data from geomagnetic satellites using traditional inversion methods has not yet been achieved. Therefore, whether traditional nonlinear inversion methods can provide relatively reliable models of tidal motion velocities remains an open question worthy of further investigation. The recently launched MSS-1 significantly enhances the observational capabilities for tidal-induced magnetic fields in low- and mid-latitude regions by providing more local time coverage. Moreover, it delivers magnetic field data with sensitivity in both east-west and north-south directions, offering a more comprehensive dataset for tidal velocity modeling.

To address this issue, this study develops a method for imaging tidal flow velocities based on tidal-induced magnetic fields observed by satellite magnetometers. This manuscript first introduces the general principles of imaging ocean flow velocities and validates the method theoretically. Subsequently, we use the M2 tidal-induced magnetic field extracted from geomagnetic satellite observation to perform tidal velocity inversion. Finally, we compare the reconstructed tidal velocity model with existing models. Our results demonstrate that satellite magnetic data can effectively measure tidal currents, potentially improving tidal models.

2. Method

Based on Maxwell's equations, the tidal-induced electric field is governed by the following equation:

$$\nabla \times \nabla \times \boldsymbol{E} + \mathrm{i}\omega\mu\sigma\boldsymbol{E} = -\mathrm{i}\omega\mu\boldsymbol{J}_s, \tag{1}$$

where $\boldsymbol{J}_s = \sigma\boldsymbol{E} + \boldsymbol{J}^{\mathrm{ext}}$ is the current source, σ presents the conductivity of the Earth, $\boldsymbol{J}^{\mathrm{ext}}$ is the tidal-induced current source, $\omega = 2\pi/T$ is the angular frequency, T denotes the tidal period, $\mathrm{i} = \sqrt{-1}$. $\mu_0 = 4\pi \times 10^{-7}$ H/m is the vacuum permeability and σ stands for the distribution of electrical conductivity. After obtaining the induced electric field, the corresponding induced magnetic field can be calculated through

$$\boldsymbol{B} = -\frac{1}{\mathrm{i}\omega}\nabla \times \boldsymbol{E}. \tag{2}$$

Accurate calculation of induced currents is essential for reliable results. Based on the theory of motional electromagnetic induction, tidal-induced current $\boldsymbol{J}^{\mathrm{ext}}$ can be expressed as:

$$\boldsymbol{J}^{\mathrm{ext}} = \frac{1}{h}\int_{a-h}^{a} \sigma_{\mathrm{ocean}}\boldsymbol{v}\,\mathrm{d}r \times \boldsymbol{B}_m, \tag{3}$$

where $\boldsymbol{v}$ represents the tidal velocity, σ_{ocean} is the seawater conductivity, and $\boldsymbol{B}_m$ denotes Earth's main magnetic field. The parameters a and h correspond to Earth's average radius (6371 km) and the maximum seawater depth, respectively. This equation highlights that tidal-induced currents depend on seawater conductivity, tidal flow velocity, and the Earth's magnetic field. Consequently, tidal-induced magnetic fields serve as a powerful method for reconstructing ocean flow velocities.

To ensure accurate modeling of tidal-induced currents and magnetic fields, we constructed a high-resolution conductivity model for the shallow Earth and adopted a 1D model (Kuvshinov et al., 2021) for the deep Earth. Additionally, the IGRF-13 model (Alken et al., 2021) was used to represent Earth's main magnetic field. The seawater conductivity model was developed using ETOPO1 seafloor topography data (Amante and Eakins, 2009), which has a spatial resolution of 1 arc-minute, in conjunction with the 15 arc-minute 3D conductivity dataset from WOA2013 (Tyler et al., 2017). To further improve the shallow Earth conductivity model, we incorporated the GlobSed sediment conductivity model (Straume et al., 2019) and the CRUST crustal conductivity model (Laske et al., 2013), forming a shallow layer with a thickness of 10 km overlying the deeper 1D conductivity structure. The final Earth conductivity model thus consists of a shallow 3D conductivity layer coupled with a deeper 1D conductivity structure. Both the Earth's conductivity model and the Earth's main magnetic field were assumed to be static, neglecting temporal variations to simplify the inversion process.

The M2 tidal-induced magnetic field analyzed in this study was derived from MSS-1, Swarm, and CryoSat observations. Specifically, we utilized vector magnetic field data from the MSS-1 satellite spanning from November 2023 to July 2024, supplemented by nearly 11 years of Swarm data and approximately 14 years of CryoSat data. First, we remove non-tidal components (e.g., main and lithospheric fields) from the observed magnetic data and select geomagnetically quiet periods (stable RC index) with low solar activity. The tidal-induced magnetic field at satellite altitude is then represented as an internal-source field using spherical harmonic coefficients, with the reference altitude aligned to MSS-1's orbital height (450 km). We calculated the spherical harmonic coefficients of the tidal-induced magnetic field through spherical harmonic expansion up to degree and order 28. For the specific details, please refer to Ren ZY et al. (2025).

To estimate the tidal flow velocities of interest, we formulated an objective function Φ_v as

$$\Phi_v = \Phi_d + \lambda\Phi_m = ||\boldsymbol{W}_d(\boldsymbol{d}_k - \boldsymbol{d}_{\mathrm{obs}})|| + \lambda||\boldsymbol{W}_m(\boldsymbol{m}_k - \boldsymbol{m}_{\mathrm{ref}})||. \tag{4}$$

In the inversion process, we specifically utilized the radial component of the tidal-induced magnetic field B_r for calculations. In Equation (4), Φ_d denotes the data misfit term, defined as the L_2-norm of the difference between synthetic response $\boldsymbol{d}_k$ and observed data $\boldsymbol{d}_{\mathrm{obs}}$. $\boldsymbol{w}_d$ is the data covariance matrix. Φ_m represents the model constraint term, which applies volume inverse-distance-square weighting parameter differences between the center and adjacent synthetic elements. $\boldsymbol{w}_m$ is the model covariance matrix.

The model parameters $\boldsymbol{m}_k$ are defined as:

$$\boldsymbol{m}_k = \log\frac{\boldsymbol{v}-\boldsymbol{v}_{\min}}{\boldsymbol{v}_{\max}-\boldsymbol{v}} \tag{5}$$

to constrain the velocity in the range $[\boldsymbol{v}_{\min}\ \boldsymbol{v}_{\max}]$, where $\boldsymbol{v}_{\min}$ and $\boldsymbol{v}_{\max}$ are corresponding to the lower and upper bound. The regularization parameter λ adjusts the trade-off between the data fitting and model constraints during inversion. By minimizing the objective function using the Limited-memory Broyden-Fletcher-Goldfarb-Shanno (L-BFGS) method (Liu DC and Nocedal, 1989), we obtained the final inverted velocity model that satisfies the required constraints.

3. Results

To assess the reliability of our inversion algorithm, we first conducted one synthetic test, comparing the inverted model with the true model. Subsequently, in the second case, we inverted the observed tidal-induced magnetic field signals extracted from geomagnetic satellite data and compared the inversion results with the currently recognized reliable HAMTIDE tide model.

3.1 Synthetic Data Inversion

The synthetic test case validates the inversion algorithm's performance using a uniform ocean current model. Case 1 represents a uniform ocean current model, of which both the real and imaginary components of ocean velocity in the north-south (θ) $\boldsymbol{V}_\theta$ and east-west (ϕ) $\boldsymbol{V}_\phi$ directions are set to 0.001 m/s. The forward modeling generated corresponding induced magnetic fields at 450 km altitude, employing a 1 degree resolution grid with 2,271,585 elements. Notably, the inversion domain comprises 563,642 unknown parameters, with each element containing 4 degrees of freedom (the real and imaginary components of the tidal velocity fields $\boldsymbol{V}_\theta$ and $\boldsymbol{V}_\phi$). The resulting induced magnetic fields were superimposed with 5% Gaussian noise to simulate the observed data. All calculations were performed on high-performance computing facilities at Central South University, utilizing Intel Xeon Gold 6248R CPUs with 48 cores.

In Case 1, the inversion procedure initialized with velocities of 0.0015 m/s for all velocity components (the real and imaginary components of $\boldsymbol{V}_\theta$ and $\boldsymbol{V}_\phi$), employing an initial regularization factor of 100 and cooling factor of 0.5. After 200 iterations, the root-mean-square (RMS) error decreased to 1.5, and the inversion converged after 347 iterations with a final RMS error of 1.13. Figure 1 compares the response of the final inversion model with the observed data. The induced magnetic field amplitudes range from 0 to 1.5 nanoteslas (nT). The observed data and the responses show a good fit with absolute errors in the real and imaginary parts not exceeding 0.5 nT. Figure 2 further compares the true velocity model (left column) with the final inversion results (right column), showing strong agreement and validating the reliability of our algorithm.

3.2 Geomagnetic Datasets Inversion

Next, we performed inversion analyses on the observed M2 tidal-induced magnetic field signals. In Case 2, we combined the tidal-induced magnetic field signals extracted from multiple satellite missions (MSS-1, Swarm, and CryoSat) to reconstruct a compre-

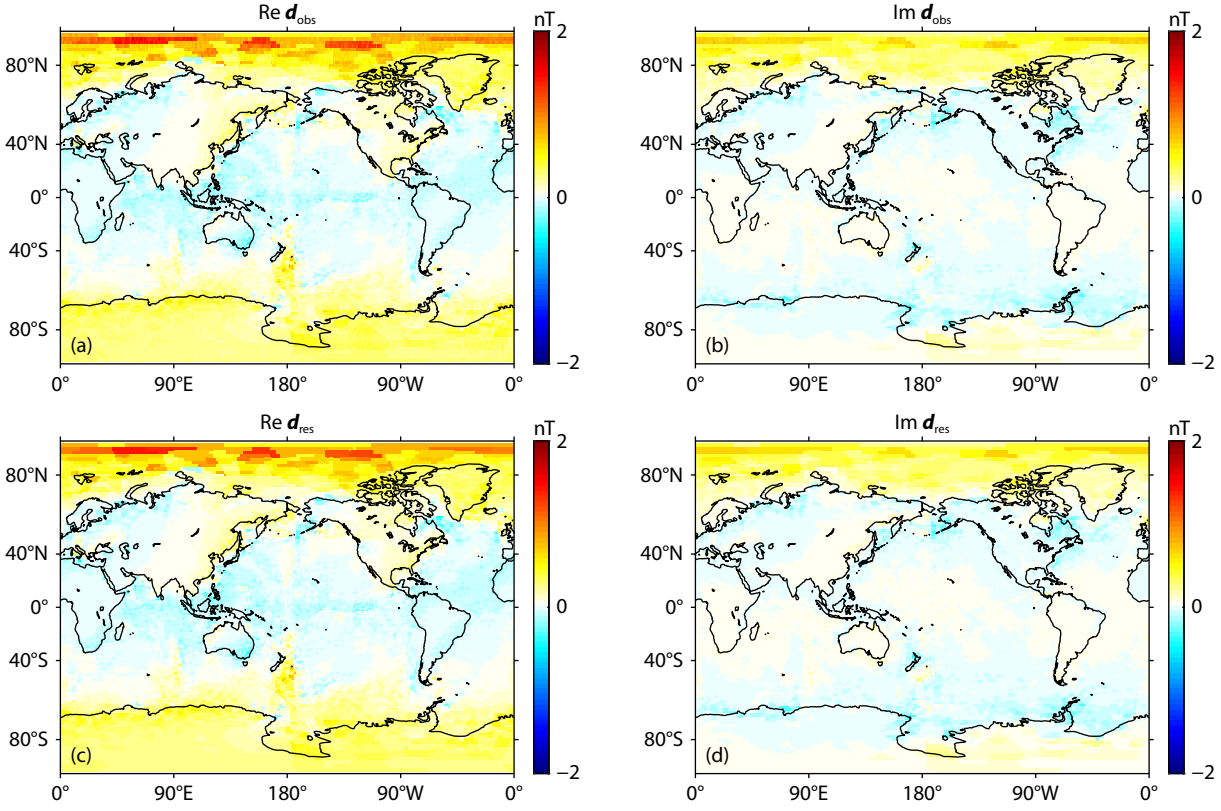

Figure 1. Comparison between observed data and theoretical responses in Case 1. (a) and (c) are real components of the observed data and responses. (b) and (d) are imaginary components of the observed data and responses.

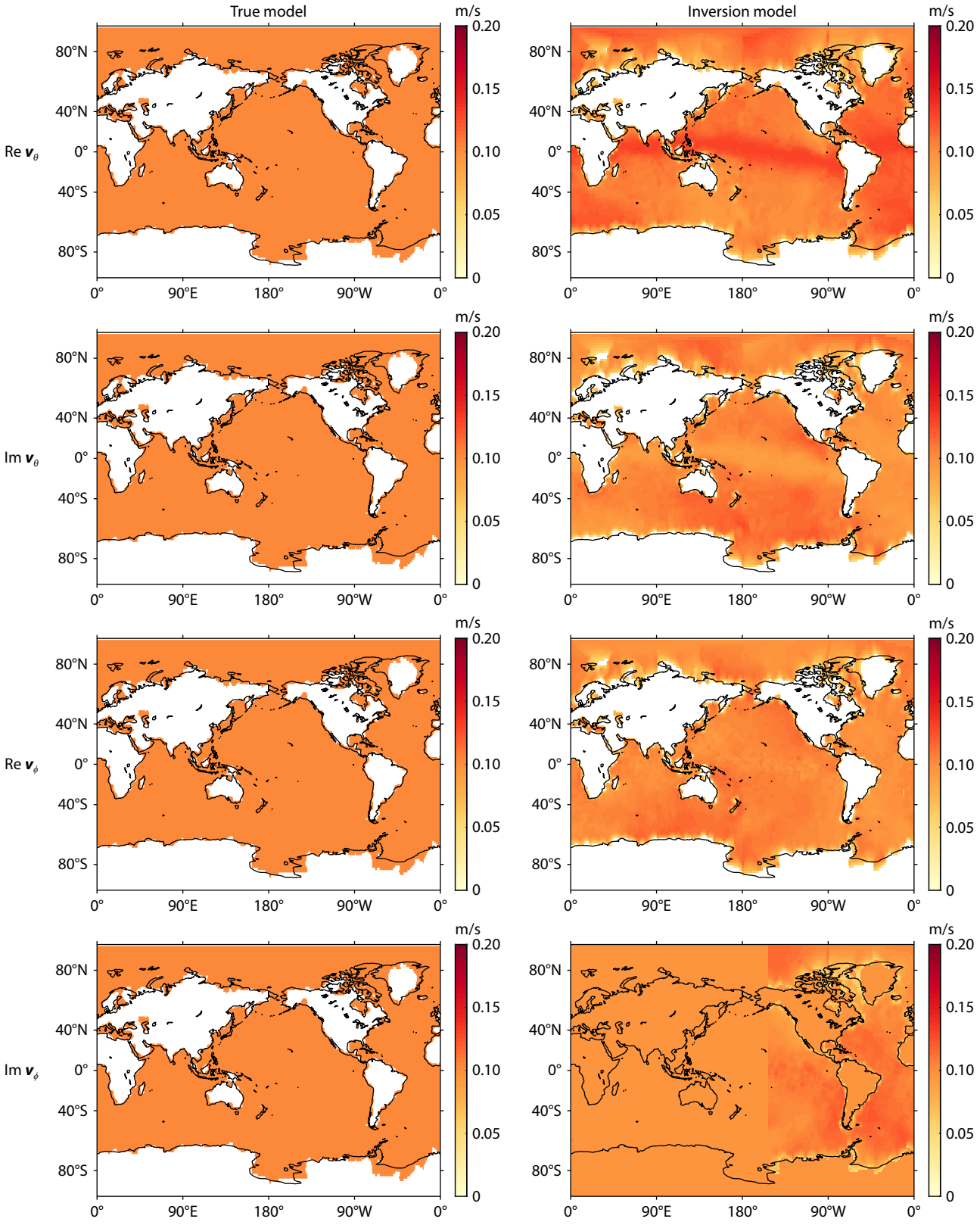

Figure 2. Comparison of the ocean flow velocity from the true model (left column) and the inverted velocity (right column) for Case 1.

hensive M2 tidal velocity model. To ensure consistency in the comparative analysis, the extracted tidal-induced magnetic signals from the geomagnetic satellites were projected to a uniform orbital altitude of 450 km , matching that of MSS-1. Except for the initial model, all inversion parameters in Case 2 remained identical to those in Case 1.

We initialized the initial model by setting both the real and imaginary components of the velocity along the θ and ϕ directions to

10^{-4} m/s. The initial RMS value was 20.16, accompanied by an error margin of 0.1 nT. After 484 iterations, the inversion terminated as the reduction in data misfit remained below the predefined threshold for several consecutive iterations, resulting in a final RMS of 10.56. In the oceanic region, the observed data and the forward response are largely consistent. However, in the continental region, the observed data display significant non-zero values, while the forward response remains nearly zero. This discrepancy is the main cause of the large termination RMS. The velocity model obtained from the inversion is generally consistent with the HAMTIDE model, though there are some differences in the maximum amplitude. This result indicates that our algorithm is capable of inverting observed tidal-induced magnetic fields to retrieve tidal velocities.

It should be noted that the HAMTIDE model provides depth-integrated velocities at fixed ocean depths throughout its computation. As a barotropic model, it represents vertically averaged motion rather than true 3D velocity profiles. This treatment inherently leads to systematic discrepancies when compared to realistic scenarios incorporating fully 3D flow dynamics and depth-dependent velocity variations. In order to develop a dependable tidal velocity model using tidal-induced magnetic field, we initiate with the HAMTIDE model as our baseline and conduct an inversion of the extracted M2 tidal-induced magnetic field from geomagnetic satellite. The initial RMS was 5.02 and the inversion converged after 41 iterations with a final RMS value of 0.996, indicating a well-constrained solution. The spatial distribution of the induced magnetic field (Figures 3) aligns closely with the response of the inversion model, further validating the reliability of the inversion. Additionally, most of the absolute errors of the induced magnetic field remain below 0.5 nT. The response generated by the inversion model shows the most considerable discrepancies with observations in the South Indian Ocean, the New Zealand region, the equatorial Pacific, and the Gulf Stream area, likely due to unresolved small-scale ocean dynamics and conductivity structures. These regional mismatches highlight where improved bathymetric constraints and higher-resolution tidal forcing could enhance model performance.

Figure 4 compares the inverted M2 tidal velocity with the HAMTIDE model, demonstrating a general agreement. Notable discrepancies are observed in high-latitude regions, whereas differences in mid-latitude areas are minimal. These findings highlight the improvements in inversion performance achieved by utilizing the M2 tidal-induced magnetic fields extracted from MSS-1, particularly in low- and mid-latitude regions. Furthermore, tests with different initial models indicate that the inversion of ocean flow velocities based on tidal-induced magnetic fields detected by geomagnetic satellites depends significantly on the initial model selection.

4. Discussion and Conclusions

This study presents a successful reconstruction of tidal flow velocities through the analysis of tidal-induced magnetic fields measured by geomagnetic satellites. Firstly, we verified the effectiveness of the inversion algorithm by employing a theoretical model. The inversion results in Case 1 are in good agreement with the true models (RMS = 1.13), demonstrating the ability of our algorithm to recover ocean flow velocity using magnetic field detected by geomagnetic satellite theoretically.

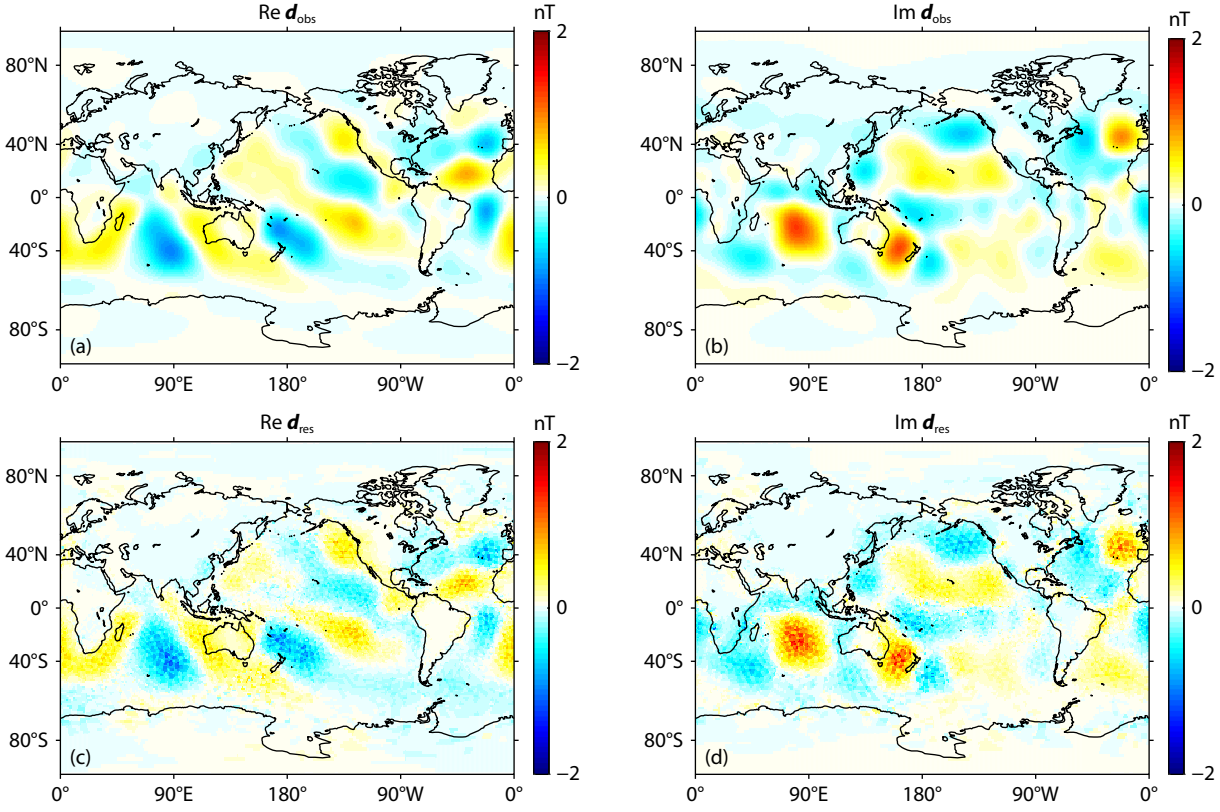

Figure 3. Similar to Figure 1, but for Case 2.

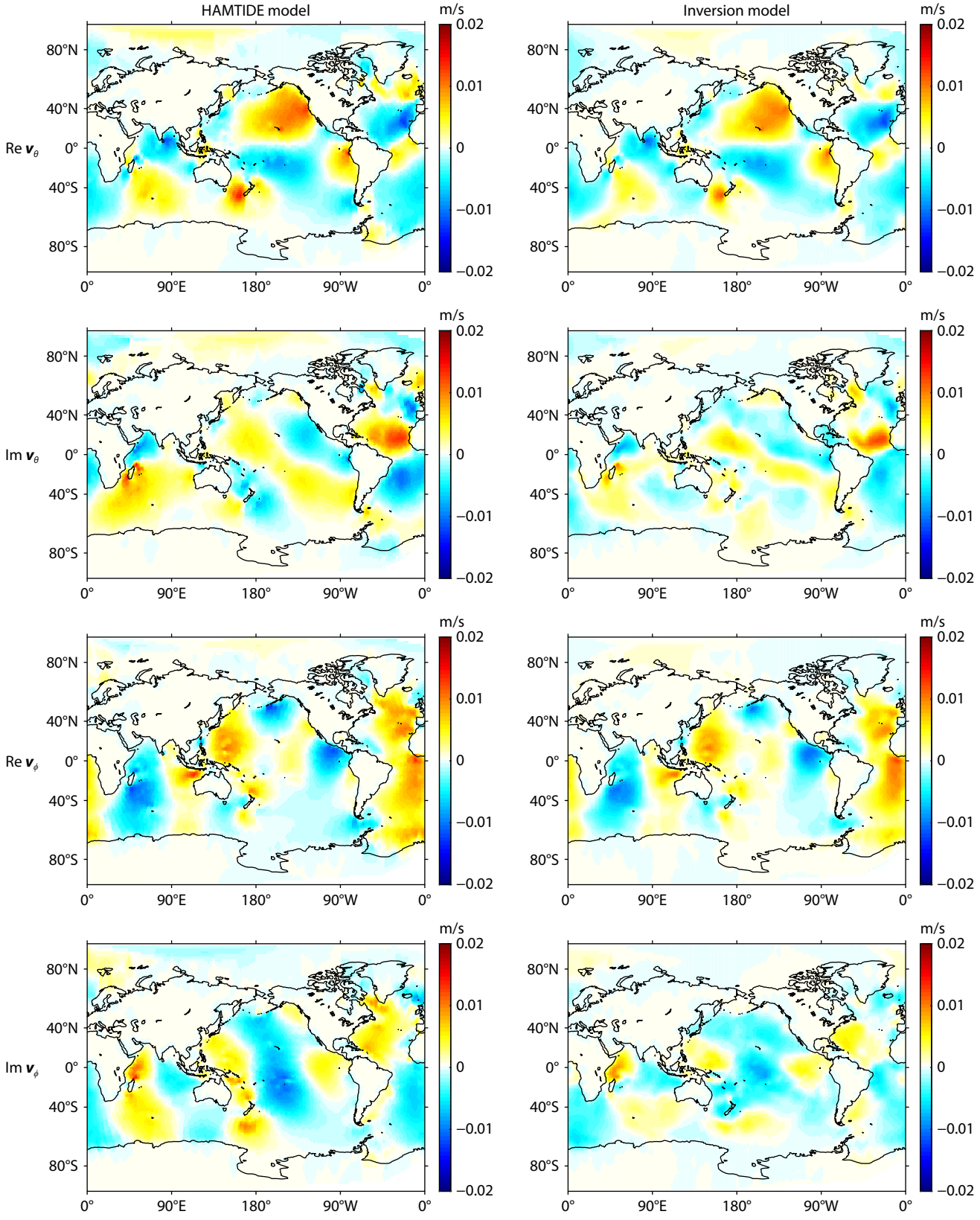

Figure 4. Comparison of the ocean flow velocity from HAMTIDE model (left column) and the inverted velocity (right column) for Case 2.

By leveraging data from MSS-1, Swarm, and CryoSat, we performed velocity inversion on the tidal-induced magnetic field signals in Case 2. Notably, the inversion process exhibited strong dependence on initial conditions - while implementations without prior information failed to converge, initializations incorporating the HAMTIDE model achieved stable solutions. Using HAMTIDE model as initial model, latitudinal variations in performance were observed: while results at low-to-mid latitudes (49°S-49°N) show

good agreement with HAMTIDE, significant discrepancies (>30% velocity differences) occur in high-latitude regions, particularly in the Southern Hemisphere beyond MSS-1's coverage. The inversion results demonstrate the feasibility of using tidal-induced magnetic field signals detected by geomagnetic satellites for imaging tidal velocities. Besides, these cases highlight the advantage of the MSS-1's low-inclination orbit (41 degrees). MSS-1 provides a broader local time coverage at low- and mid-latitudes and offers more sensitivity of induced magnetic to velocity in both the east-west directions, thereby improving the accuracy of recovering ocean tide velocity in these regions. At the same time, the influence of different initial models also indicates that our current method is strongly dependent on the selection of the initial model.

Additionally, the results establish a robust foundation for the inversion of ocean circulation velocities and contribute to the modeling of Earth's magnetic fields. As a next step, we aim to propose an iterative inversion approach that incorporates ocean circulation-induced magnetic fields into the geomagnetic model and enhances its accuracy and applicability.

Acknowledgments

This work was financially supported by the National Natural Science Foundation of China (42250102,42250101), and the Macau Foundation. We are grateful for the resources provided by the High Performance Computing Center of Central South University. We thank the European Space Agency for access to Swarm magnetic data (https://earth.esa.int/eogateway/missions/swarm/data). The MSS-1 data can be downloaded from https://mss.must.edu.mo/data.html. Data for the global bathymetric and topographic model ETOPO1 are available in NOAA, https://www.ngdc.noaa.gov/mgg/global/global.html. The IGRF-13 program for calculating the Earth's main magnetic field is sourced from NASA, https://ccmc.gsfc.nasa.gov/models/IGRF13/. The HAMTIDE tidal velocity model can be obtained from the Integrated Climate Data Center, https://icdc.cen.unihamburg.de/thredds/catalog/ftpthredds/hamtide/catalog.html.

References

Alken, P., Thébault, E., Beggan, C. D., Amit, H., Aubert, J., Baerenzung, J., Bondar, T. N., Brown, W. J., Califf, S., ... Zhou, B. (2021). International geomagnetic reference field: the thirteenth generation. *Earth Planets Space*, *73*(1), 49. https://doi.org/10.1186/s40623-020-01288-x

Amante, C., and Eakins, B. W. (2009). Etopo1 arc-minute global relief model: procedures, data sources and analysis. Boulder, Colorado: National Geophysical Data Center, NOAA.

Egbert, G. D., and Ray, R. D. (2001). Estimates of M_2 tidal energy dissipation from TOPEX/Poseidon altimeter data. *J. Geophys. Res.: Oceans*, *106*(C10), 22475–22502. https://doi.org/10.1029/2000JC000699

Finlay, C. C., Kloss, C., Olsen, N., Hammer, M. D., Tøffner-Clausen, L., Grayver, A., and Kuvshinov, A. (2020). The CHAOS-7 geomagnetic field model and observed changes in the South Atlantic Anomaly. *Earth Planets Space*, *72*(1), 156. https://doi.org/10.1186/s40623-020-01252-9

Grayver, A. V., Schnepf, N. R., Kuvshinov, A. V., Sabaka, T. J., Manoj, C., and Olsen, N. (2016). Satellite tidal magnetic signals constrain oceanic lithosphere-asthenosphere boundary. *Sci. Adv.*, *2*(9), e1600798. https://doi.org/10.1126/sciadv.1600798

Grayver, A. V., Munch, F. D., Kuvshinov, A. V., Khan, A., Sabaka, T. J., and Tøffner-Clausen, L. (2017). Joint inversion of satellite-detected tidal and magnetospheric signals constrains electrical conductivity and water content of the upper mantle and transition zone. *Geophys. Res. Lett.*, *44*(12), 6074–6081. https://doi.org/10.1002/2017GL073446

Griffiths, S. D., and Peltier, W. R. (2009). Modeling of polar ocean tides at the Last Glacial Maximum: amplification, sensitivity, and climatological implications. *J. Climate*, *22*(11), 2905–2924. https://doi.org/10.1175/2008JCLI2540.1

Knauss, J. A., and Garfield, N. (2016). *Introduction to Physical Oceanography* (3rd ed). Long Grove: Waveland Press.

Kuvshinov, A., Grayver, A., Tøffner-Clausen, L., and Olsen, N. (2021). Probing 3-D electrical conductivity of the mantle using 6 years of Swarm, CryoSat-2 and observatory magnetic data and exploiting matrix Q-responses approach. *Earth Planets Space*, *73*(1), 67. https://doi.org/10.1186/s40623-020-01341-9

Laske, G., Masters, G., Ma, Z., and Pasyanos, M. (2013). Update on crust 1.0: A 1-degree global model of Earth's crust. In *Geophysical Research Abstracts* (Vol. 15, p. 2658). Vienna, Austria: EGU.

Liu, D. C., and Nocedal, J. (1989). On the limited memory BFGS method for large scale optimization. *Math. Program.*, *45*(1), 503–528. https://doi.org/10.1007/BF01589116

Mazzega, P. (1985). M2 model of the global ocean tide derived from SEASAT altimetry. *Mar. Geod.*, *9*(3), 335–363. https://doi.org/10.1080/15210608509379532

Ray, R. D., and Mitchum, G. T. (1997). Surface manifestation of internal tides in the deep ocean: observations from altimetry and island gauges. *Prog. Oceanogr.*, *40*(1-4), 135–162. https://doi.org/10.1016/S0079-6611(97)00025-6

Ray, R. D., and Zaron, E. D. (2011). Non-stationary internal tides observed with satellite altimetry. *Geophys. Res. Lett.*, *38*(17), L17609. https://doi.org/10.1029/2011GL048617

Ren, Z. Y., Huang, Y. P., Yang, C., Chen, C. J., and Zhang, K. (2025). Preliminary results suggest observations from Macau Science Satellite-1 system can improve knowledge of tidal-induced magnetic fields. *Earth Planet. Phys.*, *9*(3), 586–594. https://doi.org/10.26464/epp2025002

Sabaka, T. J., Tyler, R. H., and Olsen, N. (2016). Extracting ocean-generated tidal magnetic signals from Swarm data through satellite gradiometry. *Geophys. Res. Lett.*, *43*(7), 3237–3245. https://doi.org/10.1002/2016GL068180

Sabaka, T. J., Tøffner-Clausen, L., Olsen, N., and Finlay, C. C. (2020). CM6: a comprehensive geomagnetic field model derived from both CHAMP and Swarm satellite observations. *Earth Planets Space*, *72*(1), 80. https://doi.org/10.1186/s40623-020-01210-5

Šachl, L., Velímský, J., Fullea, J., and Martinec, Z. (2022). Inversion of the satellite observations of the tidally induced magnetic field in terms of 3-D upper-mantle electrical conductivity: method and synthetic tests. *Geophys. J. Int.*, *229*(3), 2115–2132. https://doi.org/10.1093/gji/ggac015

Šachl, L., Knopp, O., and Velímský, J. (2024). Electrical conductivity of the suboceanic upper mantle constrained by satellite-derived tidal magnetic fields: three-dimensional inversion, validation and interpretation. *Geophys. J. Int.*, *238*(3), 1254–1268. https://doi.org/10.1093/gji/ggae209

Saynisch-Wagner, J., Baerenzung, J., Hornschild, A., and Thomas, M. (2023). Tidal transports from satellite observations of Earth's magnetic field. *Sci. Rep.*, *13*(1), 13302. https://doi.org/10.1038/s41598-023-40448-3

Schnepf, N. R., Manoj, C., Kuvshinov, A., Toh, H., and Maus, S. (2014). Tidal signals in ocean-bottom magnetic measurements of the Northwestern Pacific: observation versus prediction. *Geophys. J. Int.*, *198*(2), 1096–1110. https://doi.org/10.1093/gji/ggu190

Straume, E. O., Gaina, C., Medvedev, S., Hochmuth, K., Gohl, K., Whittaker, J. M., Abdul Fattah, R., Doornenbal, J. C., and Hopper, J. R. (2019). GlobSed: updated total sediment thickness in the world's oceans. *Geochem. Geophys. Geosyst.*, *20*(4), 1756–1772. https://doi.org/10.1029/2018GC008115

Tyler, R. H., Boyer, T. P., Minami, T., Zweng, M. M., and Reagan, J. R. (2017). Electrical conductivity of the global ocean. *Earth Planets Space*, *69*(1), 156. https://doi.org/10.1186/s40623-017-0739-7

Wunsch, C., and Stammer, D. (1998). Satellite altimetry, the marine geoid, and the oceanic general circulation. *Annu. Rev. Earth Planet. Sci.*, *26*(1), 219–253. https://doi.org/10.1146/annurev.earth.26.1.219

Yao, H. B., Xu, J. Y., Yang, C., Ren, Z. Y., and Zhang, K. (2025). A multisource geomagnetic field model incorporating ocean circulation-induced magnetic field. *Earth Planet. Phys.*, *9*(3), 550–563. https://doi.org/10.26464/epp2025029

Zhao, Z. X. (2023). Satellite evidence for strengthened M_2 internal tides in the past 30 years. *Geophys. Res. Lett.*, *50*(24), e2023GL105764. https://doi.org/10.1029/2023GL105764